

BWR STABILITY ANALYSES WITH SIMULATE-3K BENCHMARK AGAINST MEASURED PLANT DATA

Gerardo Grandi, Lotfi Belblidia, Christian Jönsson

Studsvik Scandpower, Inc.
504 Shoup Avenue, Suite 201
Idaho Falls, ID 83402

gerardo.grandi@studsvik.com, lotfi.belblidia@studsvik.com,
christian.jonsson@studsvik.com

Keywords: BWR stability analysis, CMS, SIMULATE-3K, coupled codes, validation

ABSTRACT

The best-estimate coupled neutronic/thermal hydraulics code, SIMULATE-3K (S3K), is used by many utilities, research institutes, and regulatory authorities in Europe for performing BWR stability analysis. Analysis of many measured BWR stability tests (often performed in European BWRs) provides the basis for the validation for stability parameter (decay ratio and natural frequency) calculations with S3K. This paper summarizes part of the extensive validation data base for the code, and discusses the influence of fuel pin model parameters on the stability results.

1. INTRODUCTION

S3K¹ was designed to be a best estimate tool employing a full two-group advanced nodal model and a very detailed thermal-hydraulic channel model. The underlying premise of S3K is that by modeling faithfully the detailed assembly-by-assembly neutronic and thermal-hydraulic behavior of the reactor core, S3K could be applied to many types of core transients. In particular, it is well suited for those transient in which there is a strong neutronic-thermal hydraulic coupling like BWR instabilities. In fact, S3K is capable of accurately predicting instability events.²

For BWR stability analyses, the core models were extended to include models for all major components in the BWR vessel.³ With these model extensions, S3K is fully capable of modeling BWR stability (in the time domain) with full 3-D neutronic and thermal-hydraulic capabilities. These models eliminate any need to “lump” hydraulic channels, and S3K eliminates uncertainties associated with the more traditional “engineering assumptions” often used in BWR stability analysis. Section 2 provides an overview of S3K models, with some emphasis on the fuel pin model since its effects on BWR stability will be discussed later in this paper. A description of the methodology for BWR stability analysis is provided in Section 3. Section 4 summarizes the validation of the code against measured plant data showing the applicability and accuracy of S3K for stability predictions. Finally, Section 5 discusses the influence of the fuel pin model parameters on decay ratio.

2. MODELS

The core, channel thermal hydraulic, and BWR vessel models are described in detail by Belblidia et al.⁴ A summary of these models is provided in what follows with special attention to the fuel pin model, which has not been described previously.

2.1 Core Model

The neutronic model used in S3K solves the 3-D, two-energy group, neutron diffusion equation with one or four radial nodes to represent each fuel assembly. For the BWR stability analysis 25 nodes are typically used in the axial direction to represent the active portion of each fuel assembly, and one node is used to represent the upper and lower reflectors. The S3K core model uses a fourth-order flux expansion⁵ to represent the neutron flux shape within each node (in each of the three directions). The polynomial model gives very accurate results for UO₂-fueled LWRs over a wide range of reactor types, fuel loadings, and operating conditions. Accuracy of the S3K core model depends not only on detailed 3-D neutronic and thermal-hydraulic modeling, but also on accurate representation of feedback parameters. Neutronic data is functionalized into a series of 1-D, 2-D, and 3-D table sets (for each fuel type).

2.2 Hydraulic Channel Model

The core is represented with one thermal-hydraulic channel per fuel bundle with no cross flow, because each BWR fuel bundle is surrounded by a box that precludes flow between the assemblies. The area-averaged form of the conservation equations employed in S3K is similar to that appearing in the literature.⁶ In this application, it is important to treat the dynamic momentum effects that result in the acceleration of vapor phase relative to the liquid phase. Therefore, a six-equation model is used: vapor and liquid mass conservation, vapor and liquid energy conservation. Rather than solving the separate phasic momentum equations directly, it is convenient to use the mixture momentum equation and a weighted difference of the two phasic momentum equations. The differenced momentum equation is obtained by subtracting the vapor momentum equation times one minus the void fraction from the liquid momentum equation times the void fraction.

The hydraulic primitive variable set solved for comprises phasic mass fluxes G_v and G_l , phasic enthalpies h_v and h_l , pressure P , and void fraction α . In addition to the conservation equations, closure relationships exist for each phasic density, defined as a function of the pressure and phasic enthalpy. It is important to mention that water properties are evaluated at the core exit pressure. The general drift formulation for the void fraction completes the set of equations to be solved. The concentration parameter and the void-weighted drift velocity are calculated using the EPRI correlations.⁷ The subcooled boiling model is taken from Lahey's mechanistic model.⁶

2.3 Fuel Pin Model

The heat conduction in the fuel pin is governed by the one-dimensional, radial heat conduction equation. Material properties depend on temperature and burnup. Fuel thermal conductivities for UO_2 are based on Nuclear Fuel Industries correlations as reported by Lanning et al.⁸ Fig. 1 below shows the thermal conductivity for UO_2 for four different exposures, 0, 5, 30 and 60 GWd/MT. Note that at the temperatures of interest (between 700-1000 K), there is a significant degradation of the thermal conductivity.

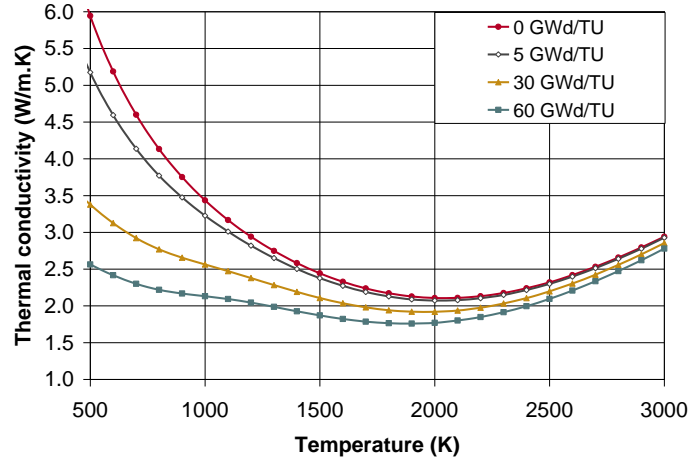


Fig. 1 UO_2 thermal conductivity as a function of temperature and exposure.

The S3K gap conductance model is based on the models of the INTERPIN code⁹ and is functionalized versus exposure and fuel temperature. The following physical effects for the gap are modeled: (a) fuel pellet cracking, (b) irradiation swelling, (c) gas gap composition changes as a result of fission gas release and (d) fuel pellet and clad thermal expansion, and (e) clad compression caused by irradiation at high pressure. It is assumed that the gap conductance is proportional to the fill gas thermal conductivity and inversely proportional to the sum of the average radial gap and the temperature jump distance for the gas:

$$h = \frac{k_g}{g + g_0} \quad (1)$$

The model does not represent explicitly the fission gas release during the life of the fuel. Instead it assumes that the gap is initially filled with helium and a degradation factor, as a function of exposure, models the degradation of the gas thermal conductivity due to fission gases. The reduction in gas conductivity is independent of the gap volume or plenum volumes, and to be proportional to the fuel volume and burnup:

$$k_g = k_{He} \left[1 - C_1 \left(\frac{Bu}{45} \right) \left(\frac{r_f}{0.51} \right) \right] \quad (2)$$

The proportionality constant, was determined using a typical BWR lattice with a fuel pin radius of 0.51 cm and an average burnup of 45 GWd/MT.

The Kjaerheim-Roldstad model¹⁰ expresses the relationship between the fraction of fuel-cladding interface in solid contact and the average radial gap:

$$\xi = C_2^{100g/r_{fp0}} \quad (3)$$

The model constant C_2 was set by the benchmarking of INTERPIN. Furthermore, the gap model assumes that there always exists a minimal residual gap, even when fuel expansion and cladding creep down might predict a closed gap. The minimum radial gap can be expressed in terms of the parameter C_2 , and the fraction of the interface in solid contact after the minimum gap has been established:

$$g_{\min} = \frac{r_{fp0}}{100} \frac{\ln(\xi_{res})}{\ln(C_2)} \quad (4)$$

Finally, the average radial gap dimension is computed using the fuel pellet radius corrected for thermal expansion and restructuring and the cladding radius corrected for compressibility and thermal expansion, as follows:

$$g = \max \left[r_{cl} - r_{fp}, g_{\min} \right] \quad (5)$$

The radial distribution of heat source is evaluated based on the pellet average exposure by interpolating in pre-computed tables generated with CASMO.¹¹ As an example, Fig. 2 below shows radial profiles for UO₂ fuel at 3 different exposures: 0, 30, and 60 GWd/MT.

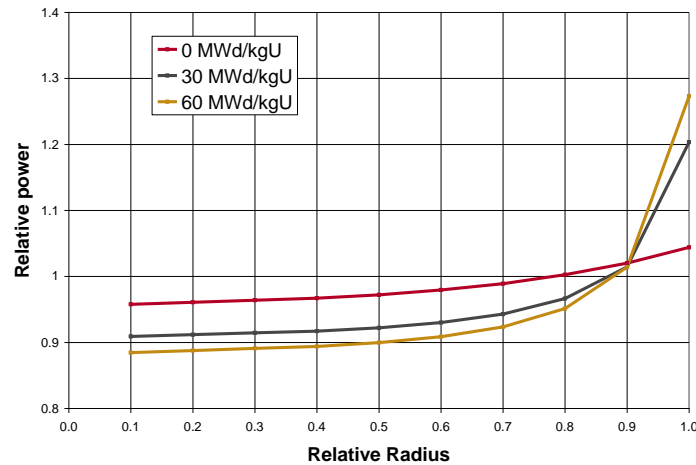


Fig. 2 Intra-pellet power profile as a function of radius and exposure.

2.4 BWR Vessel Hydraulics

The BWR vessel model is composed of upper plenum, standpipes, steam separators, bulk water region, downcomer (with 2 radial non-mixing zones), two recirculation loops, lower plenum (with 2 radial non-mixing zones), and steam dome. All BWR vessel components except the steam dome and the bulk water regions are modeled as discretized 1-D components. The steam dome and the bulk water region are lumped (single node) models. The vessel hydraulics is based on a model similar to the core channel hydraulics. Special models are included in S3K to calculate specific flow conditions. They include: (a) recirculation pumps, (b) jet pumps and (c) steam separators. The recirculation pumps, one in each of the 2 recirculation loops, drive the recirculation flow through the recirculation loops into the jet pumps or drive the core flow in a plant with internal pumps. The pump pressure rise is calculated as a function of the volumetric flow rate and speed using homologous pump curves. The pump speed may be given as a function of time or can be computed using the motor, hydraulic and friction torques. The jet pump model calculates the pump head in the internal jet pumps. All the jet pumps in one recirculation loop are lumped together. The jet pump model consists of a mixing region in which the drive flow is mixed with the suction flow and one recirculation (drive) loop containing the recirculation pump. The steam separator model takes into account the following effects: flow inertia, irreversible pressure losses, and carry under flow.

3. METHODOLOGY

S3K standard stability calculations use 24 or 25 axial neutronic and hydraulic levels and one radial node per assembly in the core (i.e. a node size of approximately 15 cm.). Each of the 1-D components in the vessel model is discretized into 50 nodes. The calculations are typically performed with neutronic time steps of 50 ms and 4 hydraulic time steps per neutronic time step (i.e. a hydraulic time step of 12.5 ms). Grandi and Smith³ discussed the effect of the temporal and spatial discretization. They found that: (a) The standard time discretization introduces a small damping effect (0.02 in decay ratio), (b) The standard axial spatial discretization has a damping effect of no more than 0.05 in decay ratio and (c) Most of the effect of the space discretization can be removed, if desired, by increasing the number of axial nodes from 24 to 48.

All three common stability modes (core-wide, regional and channel-wise oscillations) can be studied with S3K. In what follows the boundary conditions and perturbations to study each oscillation mode are described.

Global mode: The calculations are performed using the core and the BWR vessel model. The calculation starts with a pulse perturbation on the secondary side pressure. The stability parameters are computed by analyzing in the frequency domain several signals (e.g. total core power, core inlet flow, and core exit flow). The user may request the evaluation of decay ratio, natural frequency, gain, and phase using the local power range (LPRM) detector signals.

Regional mode: Core regional oscillations can be computed accurately using either only a core model if flow-pressure balance boundary conditions are imposed,³ or

the core and BWR vessel model. If the BWR vessel model is not considered, the core inlet flow is fixed and the assembly flow distribution is computed every time step to satisfy the condition that the pressure drops for all channels between the lower and upper plenum is uniform. An asymmetric perturbation in the core inlet subcooling starts the calculations. By default the stability parameters are calculated using the signals of the average power in the core octants. The user can request that the evaluation is done using the LPRM signals.

Channel mode: The steady state calculations are performed as usual to determine power, flow and density distribution in all assemblies. In the transient calculation the 3D power distribution is frozen and only core thermal hydraulic and fuel temperature calculations are performed. A pressure pulse similar to the one used to trigger the global mode starts the calculation. Results are summarized in terms of the stability parameters for the hot channel and the less stable channel. The user may request the evaluation of the stability parameters for all channels.

Specific calculations of diverging oscillations can be performed in order to evaluate the Delta over Initial CPR Vs. Oscillation Magnitude (DIVOM) slope. Depending on the reactor type either the global or the regional mode is evaluated. The result of the DIVOM evaluation is often coupled to an evaluation of the channel mode, where the maximum bundle power is defined as a key parameter in the on-line supervision of the core.

S3K numerical methods have a high computational efficiency. CPU times for global mode calculations (15 sec of simulation time), in a typical desktop computer, for a plant model with 13,654 nodes are between 310 s and 420 s. Regional mode calculations, for the same plant, take a little bit longer, between 410 s and 440 s. Channel model calculations are less expensive, no more than 200 s.

4. VERIFICATION AND VALIDATION

The qualification of S3K for stability analysis was performed by comparing its results against loop and plant data. The results are summarized in what follows.

4.1 Qualification Against Frigg Loop Data

The OF64 test section in the Frigg loop was designed as a full scale simulation of an 8x8 rod fuel assembly. Experiments were performed in 1969 on the hydraulic characteristics (stability limits) of different fuel assemblies.¹² The measurements included a wide range of operating conditions such as pressure, power, inlet subcooling, inlet throttling, and pump speed. The OF64 test section was simulated using the S3K core channel model. The balance of the experimental loop was simulated using the BWR vessel models available in S3K. Grandi and Borkowski¹³ reported the validation results of the pressure drop, void, and stability measurements. The agreement between the calculations and the experimental results is good. The bias in the predicted critical power is -7.1% and the standard deviation 3.9%. The bias in the predicted critical mass flux is +5.4% and the standard deviation 4.4%.

3.2 Qualification Against Plant Data

The S3K validation for stability analysis performed by Studsvik, includes analyses of the following plants: Ringhals-1, cycles 14 – 17,¹⁴ Oskarshamn-3, cycles 7 – 17,¹⁵ Olkiluoto-1, cycles 18-26,¹⁶ Leibstadt, cycle 19¹⁷. Validation against measurements in German plants is not part of the Studsvik benchmark database but is discussed by Gorzel et al.¹⁸

Ringhals-1 reactor is of ASEA ATOM design with external recirculation pumps. Stability measurements were performed in BOC 14, 15, 16 and 17. These measurement campaigns were the basis for the NEA/OECD Stability Benchmark. S3K results for the Ringhals-1 stability benchmark were analyzed in detail by Grandi and Smith.³ Table 1 summarizes those results in terms of decay ratio and natural frequency.

Table 1 Ringhals-1 stability results

Cycle	Case	Power (%)	Flow (%)	Measurement		S3K		Differences		
				Decay Ratio	Frequency	Decay Ratio	Frequency	Decay Ratio	Frequency	
14	1	65.0	35.6	0.30	0.43	0.28	0.46	-0.02	0.03	
14	3	65.0	31.8	0.69	0.43	0.50	0.43	-0.19	0.00	
14	4	70.0	31.7	0.79	0.55	0.71	0.53	-0.08	-0.02	
14	5	70.0	33.5	0.67	0.51	0.64	0.52	-0.03	0.01	
14	6	70.2	35.8	0.64	0.52	0.57	0.52	-0.07	0.00	
14	7	75.1	33.7	0.78	0.52	0.73	0.51	-0.05	-0.01	
14	9	72.6	32.0	0.80	0.56	0.75	0.55	-0.05	-0.01	
14	10	77.7	35.6	0.71	0.50	0.67	0.52	-0.04	0.02	
15	1	64.7	35.9	0.23	0.44	0.32	0.48	0.09	0.04	
15	2	65.2	33.7	0.24	0.42	0.30	0.46	0.06	0.04	
15	3	65.1	31.6	0.21	0.43	0.37	0.45	0.16	0.02	
15	4	70.1	36.1	0.33	0.44	0.39	0.49	0.06	0.05	
15	5	70.1	34.2	0.43	0.44	0.44	0.48	0.01	0.04	
15	6	70.1	34.2	0.59	0.47	0.55	0.48	-0.04	0.01	
15	8	75.2	34.6	0.77	0.55	0.66	0.54	-0.12	-0.01	
15	9	71.1	31.5	0.67	0.53	0.69	0.54	0.02	0.01	
15	10	77.3	36.6	0.60	0.54	0.63	0.55	0.03	0.01	
16	1	64.3	35.7	0.54	0.48	0.52	0.48	-0.02	0.00	
16	2	64.6	34.0	0.54	0.48	0.57	0.48	0.03	-0.01	
16	3	64.6	32.1	0.69	0.47	0.64	0.46	-0.05	-0.01	
16	4	70.2	37.0	0.71	0.52	0.61	0.51	-0.10	-0.02	
16	5	69.9	34.1	0.67	0.49	0.67	0.49	0.00	0.00	
16	6	69.5	31.8	0.79	0.49	0.72	0.47	-0.07	-0.02	
16	7	74.4	35.4	0.72	0.50	0.67	0.50	-0.05	0.00	
16	8	74.9	33.9	0.82	0.49	0.73	0.49	-0.09	0.00	
16	9	74.6	31.9	0.87	0.48	0.79	0.47	-0.08	-0.01	
16	10	76.0	36.6	0.65	0.50	0.63	0.50	-0.02	0.00	
16	11	66.1	31.7	0.66	0.48	0.71	0.49	0.05	0.01	
17	2	65.6	34.3	0.24	0.46	0.31	0.59	0.07	0.13	
17	4	69.5	36.1	0.32	0.46	0.30	0.63	-0.02	0.17	
17	5	69.9	34.8	0.28	0.42	0.23	0.59	-0.05	0.17	
17	6	69.7	32.6	0.34	0.46	0.22	0.51	-0.12	0.05	
17	7	74.9	35.9	0.33	0.46	0.25	0.53	-0.09	0.07	
17	8	75.1	34.9	0.41	0.48	0.29	0.50	-0.12	0.02	
17	9	75.4	32.4	0.57	0.47	0.47	0.47	-0.10	0.00	
17	10	78.1	35.2	0.49	0.49	0.39	0.49	-0.10	0.00	
								Bias	-0.03	0.02
								Std Dev	0.07	0.05

There is good agreement between the measured and calculated stability parameters. Decay ratios are computed with a bias of -0.03 and a standard deviation of 0.07. Frequencies are predicted with a bias of +0.02 and a standard deviation of 0.05.

Oskarshamn-3 and Olkiluoto-1 reactors are of ASEA-ATOM design with internal recirculation pumps. Table 2 and 3 summarize the S3K results in terms of decay ratio and natural frequency for Oskarshamn-3 and Olkiluoto-1 respectively. It is interesting to note that many of the Olkiluoto-1 measurements were performed at MOC conditions.

Table 2 Oskarshamn-3 stability results

Cycle	Case	Power(%) Flow (%)		Measurement		S3K		Difference	
				Decay Ratio	Frequency	Decay Ratio	Frequency	Decay Ratio	Frequency
7	1	66.0	34.0	0.61	0.50	0.63	0.53	0.02	0.03
7	2	69.6	33.0	0.78	0.49	0.71	0.52	-0.07	0.03
7	3	73.0	32.6	0.87	0.50	0.78	0.51	-0.09	0.01
7	4	69.3	33.0	0.86	0.50	0.76	0.53	-0.10	0.03
7	5	72.5	32.8	0.95	0.50	0.81	0.53	-0.14	0.03
7	6	61.9	29.6	0.86	0.47	0.86	0.50	0.00	0.03
7	7	61.1	29.5	0.93	0.46	0.85	0.49	-0.08	0.03
7	8	72.2	37.5	0.67	0.54	0.58	0.57	-0.09	0.03
7	9	77.6	37.2	0.81	0.54	0.65	0.56	-0.16	0.02
10	3	74.7	48.8	0.31	0.66	0.54	0.75	0.23	0.09
10	5	59.8	33.5	0.67	0.53	0.74	0.59	0.06	0.05
10	7	56.4	31.2	0.71	0.50	0.78	0.56	0.07	0.06
10	8	60.2	33.2	0.77	0.52	0.77	0.57	0.00	0.05
11	1	63.4	33.8	0.72	0.52	0.76	0.58	0.04	0.06
11	2	60.5	33.4	0.70	0.56	0.86	0.60	0.16	0.04
12	1	62.7	33.3	0.68	0.51	0.71	0.56	0.02	0.05
12	2	62.5	33.3	0.83	0.55	0.82	0.58	-0.01	0.03
13	1	65.3	36.6	0.69	0.51	0.64	0.59	-0.05	0.08
13	3	65.0	38.9	0.63	0.49	0.59	0.58	-0.04	0.09
14	1	50.0	38.0	0.32	0.50	0.32	0.55	0.00	0.05
14	2	50.0	40.8	0.30	0.49	0.33	0.56	0.03	0.07
14	3	66.2	38.8	0.63	0.57	0.64	0.66	0.01	0.09
14	4	66.0	38.2	0.61	0.57	0.67	0.65	0.06	0.08
14	5	66.8	41.2	0.53	0.54	0.46	0.63	-0.07	0.09
14	7	48.0	29.2	0.99	0.54	0.95	0.57	-0.04	0.03
14	8	67.0	41.0	0.67	0.58	0.72	0.67	0.05	0.09
15	1	75.0	47.6	0.54	0.57	0.54	0.70	0.00	0.13
15	2	71.0	46.1	0.45	0.55	0.53	0.68	0.08	0.13
16	1	48.0	34.4	0.55	0.50	0.56	0.53	0.01	0.03
16	2	75.0	48.9	0.25	0.53	0.39	0.71	0.14	0.18
17	1	53.4	35.1	0.68	0.55	0.52	0.59	-0.16	0.04
17	2	80.3	51.2	0.36	0.64	0.42	0.75	0.06	0.11
Bias								0.00	0.06
Std. dev.								0.09	0.04

Table 3 Olkiluoto-1 stability results

Cycle	Case	Power (%)	Flow (%)	Measurement		S3K		Difference	
				Decay Ratio	Frequency	Decay Ratio	Frequency	Decay Ratio	Frequency
18	boc-18a	53.5	38.5	0.47		0.51	0.54	0.04	
18	boc-18-b	56.4	38.2	0.58		0.55	0.54	-0.03	
18	boc-18-c	57.5	38.1	0.69		0.56	0.54	-0.13	
20	boc-20-1	70.1	48.1	0.22		0.31	0.58	0.09	
20	moc-20-2	68.1	48.6	0.30		0.43	0.66	0.13	
20	moc-20-3	67.6	48.5	0.38		0.40	0.60	0.02	
21	boc-21-1	66.6	48.7	0.15		0.29	0.57	0.14	
21	moc-21-2	67.3	48.4	0.39		0.42	0.67	0.03	
21	moc-21-3	67.8	48.9	0.39		0.46	0.64	0.07	
22	boc-22-1	65.1	48.6	0.19		0.25	0.46	0.06	
22	moc-22-2	67.1	48.5	0.34		0.39	0.65	0.05	
23	moc-23-2	67.4	48.7	0.39		0.39	0.67	0.00	
24	boc-24-1	67.1	47.8	0.29		0.31	0.61	0.02	
24	moc-24-2	67.0	47.5	0.43		0.40	0.62	-0.03	
24	moc-24-3	66.3	48.2	0.60		0.52	0.68	-0.08	
24	moc-24-4	67.1	48.0	0.42		0.38	0.59	-0.04	
25	moc-25-2	66.0	48.0	0.27		0.33	0.61	0.06	
25	moc-25-3	67.4	47.7	0.45		0.48	0.66	0.03	
26	moc-26-1	67.3	48.6	0.58		0.51	0.68	-0.07	
26	moc-26-2	67.0	48.5	0.55		0.47	0.63	-0.08	
								Bias	0.01
								Std. dev.	0.07

Oskarsham-3 decay ratios are computed with a bias of +0.00 and a standard deviation of 0.09. Frequencies are predicted with a bias of +0.06 and a standard deviation of 0.04. Olkiluoto-1 decay ratios are computed with a bias of +0.01 and a 0.07 standard deviation.

Of particular interest to the US BWR operators are the measurements at Leibstadt. These measurements are part of the NACUSP project¹⁹, and have three interesting features: (a) Measured data are scarce for jet pump plants, (b) The cycle 19 core is loaded with assemblies of the last generation design (10x10 fuel with partial length rods), and (c) Traversing In-Core Probe (TIP) measurements were performed in four representative channels during the stability measurements. TIP comparisons at such power/flow conditions are not common and provide valuable information for code validation. Belblidia et al.²⁰ show a comparison of the S3K results against TIP and stability measurements. Table 4 summarizes the S3K results in terms of decay ratio and natural frequency.

Table 4 Leibstadt stability results

Cycle	Case	Power (%)	Flow (%)	Measurement		S3K		Differences		
				Decay Ratio	Frequency	Decay Ratio	Frequency	Decay Ratio	Frequency	
19	1	72.3	51.2	0.43	0.68	0.45	0.64	0.02	-0.04	
19	3	74.3	48.9	0.46	0.67	0.54	0.64	0.08	-0.03	
19	4	74.2	49.2	0.55	0.70	0.57	0.66	0.02	-0.04	
19	5	59.6	44.9	0.49	0.65	0.54	0.64	0.05	-0.02	
19	6	70.0	44.6	0.68	0.66	0.71	0.61	0.03	-0.05	
19	7	54.5	41.4	0.59	0.63	0.59	0.61	0.00	-0.02	
19	8	61.1	41.0	0.71	0.63	0.73	0.59	0.02	-0.04	
19	9	35.1	36.1	0.40	0.47	0.30	0.44	-0.10	-0.04	
19	10	47.6	36.2	0.64	0.59	0.57	0.56	-0.07	-0.03	
19	11	43.1	36.1	0.54	0.54	0.48	0.52	-0.06	-0.02	
								Bias	0.00	-0.03
								Std. dev.	0.06	0.01

The bias in the decay ratio is +0.00 and the standard deviation 0.06. The natural frequencies are computed with a bias of -0.03 and a standard deviation of 0.01.

Figures 3 and 4 summarize the results of the validation in terms of the global decay ratio and natural frequency for all plants. Decay ratios have a bias of +0.00 and a standard deviation is 0.09. Frequencies have a bias of +0.03 and a standard deviation of 0.05.

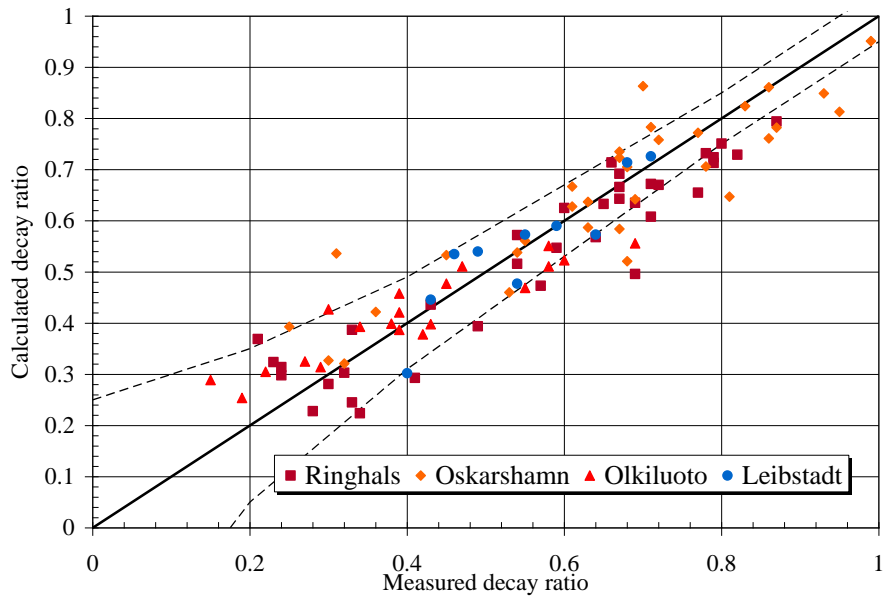


Fig. 3 Global decay ratios comparison for all plants

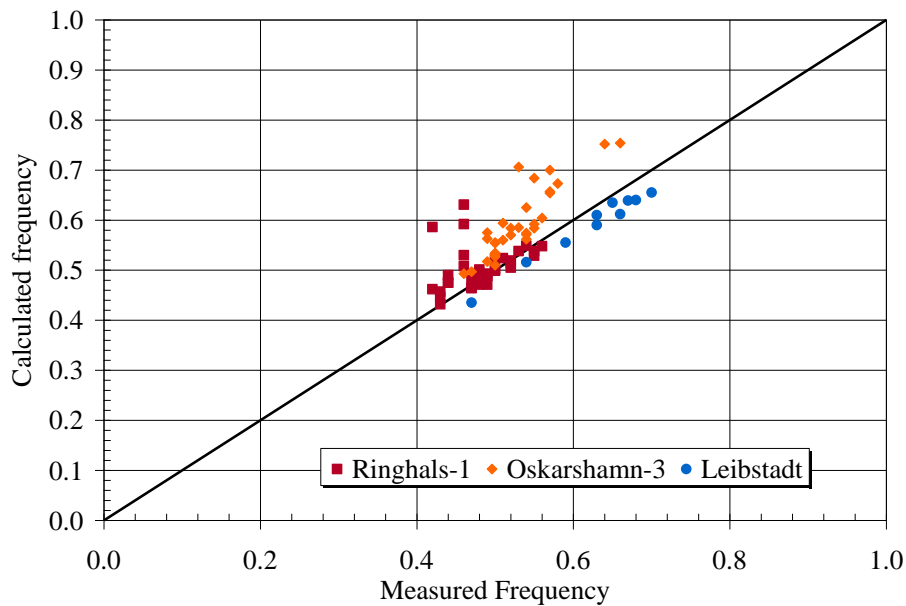


Fig. 4 Natural frequency comparison for all plants

Summarizing, S3K has been validated for plants of different design: internal, external, and jet pump plants constructed by different vendors GE, ASEA-ATOM, KWU for conditions close and in many cases inside the exclusion region. Measurements include both BOC and MOC conditions. The validation work performed by Studsvik (and other organizations) clearly shows that S3K is capable of performing BWR stability analysis. However, plant specific validation is needed if accurate predictive results are to be obtained. This statement is valid for S3K or any other code used for BWR stability evaluations.

5. EFFECT OF FUEL PIN MODEL ON STABILITY PARAMETERS

Simplified theoretical (reduced-order) models like the one developed by Lange et al.²¹ provide deep insight into the nonlinear behavior of the BWR systems. However, some of approximations used in these models may neglect important 3D effects that exist in real BWR cores, such as the effect of a non-uniform exposure distribution. The effect of the 3D exposure distribution on the fuel pin material properties as well as intra-pellet power distribution and its impact on stability predictions are discussed in this section.

For this study three cases of the cycle 23 predictive calculations for Leibstadt²⁰ were chosen. All cases have the same power and flow conditions (62.3% power, 45% flow), but differ in their core life: BOC (25 GWd/MT), MOC (30.7 GWd/MT), and EOC (35.5 GWd/MT).

To understand the effect of the different sub-models of the fuel pin model it is convenient to define the fuel time constant:

$$\theta_f \propto \frac{(\rho c_p)_f r_f}{\frac{k_f}{r_f} + \frac{k_g}{\max\{(r_{cl} - r_{fp}), g_{\min}\} + g_0}} \quad (6)$$

And remember that, for present fuel designs, a smaller time constant has a destabilizing effect. So any sub-model that increase the fuel thermal conductivity or the gap conductance has a destabilizing effect. The degradation of the thermal conductivity or gap conductance has a stabilizing effect.

5.1 Effect of the Fuel Thermal Conductivity Sub-model

Two sets of calculations were performed: in the first one, the fuel thermal conductivity degradation was taken into account (see Fig. 1); in the second set the degradation was neglected. Table 5 below summarizes the results. If the fuel thermal conductivity is neglected, the fuel time constant is decreased, and the decay ratios increased. Comparing the differences in the third row, one observes that the destabilizing effect increases (slightly) with exposure.

Table 5: Effect of the Fuel Thermal Conductivity Degradation

	BOC		MOC		EOC	
	Decay Ratio	Natural Frequency	Decay Ratio	Natural Frequency	Decay Ratio	Natural Frequency
With Degradation	0.67	0.68	0.73	0.68	0.73	0.60
No Degradation	0.72	0.68	0.79	0.68	0.81	0.60
Difference	0.05	0.00	0.06	0.00	0.07	0.00

5.2 Effect of the Gap Conductance Sub-model

The effect of exposure on the gap conductance has two competing effects. Higher exposures imply lower gas thermal conductivity due to fission gas release (stabilizing effect), but smaller gap widths due to fuel restructuring (destabilizing effect). The first effect is governed by constant C_l on Eq. (2), and the second one by the residual fraction of the interface in solid contact (ζ_{res}) on Eq. (4) and the gap width at cold conditions.

Two sets of calculations were performed to analyze the effect of the fission gas release: in the first set, the thermal conductivity degradation was taken into account using Eq. (2); in the second set the gap was assumed to be filled with helium during its entire life (i.e. no fission gas release). Table 6 below summarizes the results. As expected neglecting the fission gas release has a destabilizing effect. However, the effect predicted by S3K is small.

Table 6: Effect of the Gas Thermal Conductivity Degradation

	BOC		MOC		EOC	
	Decay Ratio	Natural Frequency	Decay Ratio	Natural Frequency	Decay Ratio	Natural Frequency
With Fission Gas Release	0.67	0.68	0.73	0.68	0.73	0.60
No Fission Gas Release	0.68	0.68	0.75	0.68	0.75	0.61
Difference	0.01	0.00	0.02	0.00	0.02	0.01

The effect of the gap width was evaluated by modifying the residual fraction of the interface in solid contact. Two sets of calculations were performed: in the first set, 50% of the interface is assumed to be in solid contact once the gap has been closed ($\zeta_{res}=0.50$); in the second set the fraction was decreased to 9.5% ($\zeta_{res}=0.095$). The minimum residual gaps computed by Eq. (4) are 0.0022 cm and 0.0075 cm respectively. Note that the cold dimensions for the fuel pins present in the core are between 0.0075 cm and 0.0090 cm. So, for all practical purposes, fresh fuel cold dimensions are used in the second set of calculations. Both the fuel restructuring and the thermal expansion are ignored. Table 7 below summarizes the results. If the minimum residual gap is increased, the fuel time constant becomes bigger which introduces a significant stabilizing effect.

Table 7: Effect of the Solid Contact Fraction / Gap dimension

	BOC		MOC		EOC	
	Decay Ratio	Natural Frequency	Decay Ratio	Natural Frequency	Decay Ratio	Natural Frequency
Contact Fraction 0.50 Minimum Gap 0.0022 cm	0.67	0.68	0.73	0.68	0.73	0.60
Contact Fraction 0.094 Minimum Gap 0.0075 cm	0.47	0.62	0.51	0.62	0.52	0.55
Difference	-0.21	-0.06	-0.23	-0.06	-0.21	-0.06

The net effect of the two competing phenomena described above was evaluated by analyzing two sets of calculations: in the first set the gap conductance is computed assuming burned fuel (i.e. gas thermal conductivity degradation and gap closure due to fuel restructuring); in the second set the gap conductance was computed assuming fresh fuel (i.e. no thermal conductivity degradation and fresh fuel hot dimensions for the gap). Table 8 below summarizes the results. As expected from the previous results (Tables 6 and 7), the gap width stabilizes the fresh fuel calculations.

Table 8: Effect of Gap Conductance

	BOC		MOC		EOC	
	Decay Ratio	Natural Frequency	Decay Ratio	Natural Frequency	Decay Ratio	Natural Frequency
Fission Gas Release and Fuel Restructuring	0.67	0.68	0.73	0.68	0.73	0.60
No Fission Gas Release and Hot Gap Dimensions	0.59	0.65	0.65	0.64	0.64	0.57
Difference	-0.08	-0.03	-0.09	-0.04	-0.10	-0.04

5.3 Effect of the Intra-pellet Power Shape Sub-model

Two sets of calculations were performed: in the first set, the power profiles shown in Fig. 2 above were used; in the second set a flat profile was used. Table 9 below summarizes the results. The flat intra-pellet power distribution predicts larger fuel temperatures in steady state. This is equivalent to a decrease in the fuel thermal conductivity, which increases the fuel time constant and stabilizes the results.

Table 9: Effect of Intra-Power Profiles

	BOC		MOC		EOC	
	Decay Ratio	Natural Frequency	Decay Ratio	Natural Frequency	Decay Ratio	Natural Frequency
CASMO Profile	0.67	0.68	0.73	0.68	0.73	0.60
Flat Profile	0.64	0.66	0.69	0.67	0.68	0.59
Difference	-0.04	-0.02	-0.04	-0.01	-0.05	-0.02

Summarizing, the effects of the different parameters of the fuel pin model have been assessed for in-phase oscillations. Fuel thermal conductivity degradation with exposure has a significant destabilizing effect. On the other hand, neglecting the fuel restructuring as a function of exposure and the variation of intra-pellet power profile with exposure may lead to non-conservative results due to the significant stabilizing effect. Note that changes of the pellet and cladding dimension are more important, with regard to gas gap heat transfer, than the gas thermal conductivity degradation.

6. CONCLUSIONS

S3K provides a very flexible and accurate tool for BWR stability analysis. The qualification results against plant data allow us to conclude that decay ratios and natural frequencies are well predicted by S3K. The accuracy of the calculations can be quantified close to the exclusion region by the average bias (+0.00) and the standard deviation (0.08). It is the authors' experience that accurate predictive calculations are possible with S3K if plant specific validation is performed, and the conditions for the prediction do not differ significantly from those in validation database. Plant power upgrades, outside of the present validation data base, or the loading of assemblies with significant differences in the hydraulic characteristics compared to the ones present in the validation require an extension of the database.

Since S3K tracks in detail fuel pins in the core (using a pin-power reconstruction method) and is capable of performing full thermal-margin calculations, the capabilities for stability analysis can be combined with 3D transient CPR methodology proposed by Jönsson et al.^{22, 23} resulting in a unique tool to compute DIVOM curves.

Despite of the fact that of the full 3-D neutronic and thermal-hydraulic capabilities (in the time domain), S3K numerical methods have a high computational efficiency that allows its use to predict the stability parameters in the BWR core surveillance system GARDEL.²⁴

NOMENCLATURE

Bu	Local exposure (MWd/kgU)
C_1	Gas conductivity degradation constant
C_2	Constant of the Kjaerheim-Roldstad model
h	Gap conductance
k	Fuel pellet thermal conductivity
g	Average radial gap
g_{\min}	Minimum residual gap
g_0	Temperature jump distance for the gap
k_g	Filling gas thermal conductivity
k_{He}	Helium thermal conductivity
$r_{fp,0}$	Fuel pellet radius without corrections
r_{fp}	Fuel pellet radius corrected for thermal expansion and restructuring

r_{cl}	Clad inner radius corrected for compressibility and thermal expansion
ξ	Fraction of fuel-cladding interface in solid contact
ξ_{res}	Fraction of fuel-cladding interface in solid contact after minimum gap

ACKNOWLEDGMENTS

The authors would like to acknowledge Kernkraftwerk Leibstadt, OKG, and Teollisuuden Voima OY for allowing us to use the stability measurements at their plants for this work.

REFERENCES

1. J. BORKOWSKI, et al., "Best-estimate Three-Dimensional Transient Analysis Using Design-basis Methodology," *International Meeting on Best-Estimate Methods in Nuclear Installation Safety Analysis (BE-2000)*, Washington, D.C., November (2000).
2. M. KRUNERS, "Analysis of Instability Event in Oskarshamn-3, Feb. 8, 1998, with SIMULATE-3K," SKI Report 98:42, Statens Kärnkraftinspektion, SE-10658, Stockholm (1998).
3. G. GRANDI, K. S. SMITH, "BWR Stability Analysis with SIMULATE-3K," *Proceedings Int. Conf. New Frontiers of Nuclear Technology (PHYSOR 2002)*, Seoul, Korea, October 7 - 10 (2002).
4. L. A. BELBLIDIA, et al., "SIMULATE-3K Peach Bottom 2 Turbine Trip 2 Benchmark Calculations", *Nucl. Sci. Eng.*, **148**, 325 (2004).
5. K. S. SMITH, "QPANDA: An Advanced Nodal Method for LWR Analysis," *Trans. Am. Nucl. Soc.*, **50**, 532 (1985).
6. R. T. LAHEY and F. J. MOODY, *The Thermal-Hydraulics of a Boiling Water Reactor*, American Nuclear Society (1993).
7. G. LELLOUCHE, B. ZOLOTAR, "Mechanistic Model for Predicting Two-Phase Void Fraction for Water in Vertical Tubes, Channels and Rod Bundles", EPRI NP-2246-SR (1982).
8. D. D. LANNING, et al., "FRAPCON-3 Updates," NUREG/CR-6534, Vol. 4, PNL-11513 (2005).
9. G. GRANDI, D. HAGRMAN, "Improvements to the INTERPIN Code for High Burnup and MOX Fuel," *Trans. Am. Nuc. Soc.* **97**, 614-615 (2007).
10. G. KJAERHEIM and E. ROLSTAD, "In-Pile Determination of UO₂ Thermal Conductivity, Density Effect, and Gap Conductance," HWR-80, Halden, Norway (1967).

11. Z. XU, Private communication (2007).
12. R. EKLUND, O. NYLUND, A. JENSEN, "OF-64. Hydraulic Characteristics and Stability Limits," FRIGG PM-68, Asea Atom, February (1970).
13. G. GRANDI, J. BORKOWSKI, "Benchmark of SIMULATE-3K Against the Frigg Loop Stability Experiments," *Proceedings of Advances in Nuclear Fuel Management III (ANFM III)*, Hilton Head, South Carolina, USA, October 5-8 (2003).
14. T. LEFVERT, "OECD/NEA Nuclear Science Committee BWR Stability Benchmark, Volume 1, Final Specifications," Rev. 1, October (1994).
15. C. NETTERBRANT, OKG Reports, Reg. No. 2000-03039 dated 2000-03-16; Reg. No. 3/P20/152, dated 2000-08-25; Reg. No. 3/P20-/160, dated 2001-07-09.
16. T. HÄMÄLÄINEN, "OL1/OL2- Stability Measurement Analysis," TVO Report 120863 (2007).
17. C. AGUIRRE, "KKL C19 Core Stability Test after Power Uprate," KKL Technischer Bericht BET/02/128 (2003).
18. A. GORZEL, et al., "Simulation of Neutronic-Thermal Hydraulic Oscillations Observed During Stability Tests at German Boiling Water Reactors," *The 11th International Topical Meeting on Nuclear Reactor Thermal-Hydraulics (NURETH-11)*, Avignon, France, October 2-6 (2005).
19. C. AGUIRRE, et al., "Natural Circulation and Stability Performance of BWRs (NACUSP)," *Nucl. Eng. Des.*, **235**, 423 (2005).
20. L. BELBLIDIA, et al., "SIMULATE-3K Stability Benchmarking and Predictive Calculations of Leibstadt," *Proceedings Int. Conf. Nuclear Power a Sustainable Resource (PHYSOR 2008)*, Interlaken, Switzerland, September 14-19 (2008).
21. C. LANGE, et al., "In Depth Analysis Of The Nonlinear Stability Behavior Of BWR-System," *Proceedings Int. Conf. Nuclear Power a Sustainable Resource (PHYSOR 2008)*, Interlaken, Switzerland, September 14-19 (2008).
22. C. JÖNSSON, et al., "Cycle Specific BWR Reload Analysis Using SIMULATE-3K", *Proceedings of Advances in Nuclear Fuel Management IV (ANFM IV)*, Hilton Head, South Carolina, USA, April 12-15 (2009).
23. C. JÖNSSON, "Analysis of Regional Oscillations and DIVOM Curves", (in Swedish)," Technical Report SSP-06/118 (2006).
24. A. NOËL, D. DEAN, "GARDEL BWR On-line Monitoring Experience at Cooper and Monticello," *Trans. Am. Nucl. Soc.* **97**, 737-738, November (2007).